X-Ray Diffraction

Equipment

- Tel-X-ometer x-ray spectrometer
- LiF crystal diffraction grating
- Geiger counter detector
- 1mm and 3mm lead collimator slides
- Tel-Atomic Digicounter digital pulse counter
- X-ray tube current monitoring cable
- Fluke multimeter
- Acrylic plastic x-ray attenuator slide plate

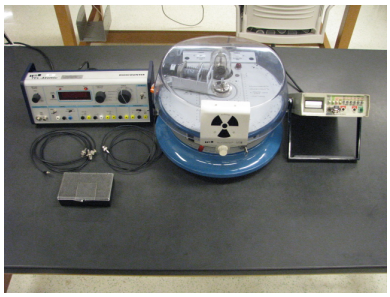

Figure 1: A photograph of the experimental setup.

Preparation

Review the place of x-rays in the electromagnetic spectrum. Understand how a diffraction grating works in an optical spectrometer. Know the Planck energy relation for a quantum of light.

Goals of Experiment

- Introduction to x-ray crystallography.
- To understand how x-rays are produced and to examine the hypothesis that they are electromagnetic radiation.
- To understand the source of k-shell x-rays.
- To get experience with the control and measurement of x-rays and to work with a spectrometer that operates in the x-ray region of the electromagnetic spectrum.

Theory

In the late 19th century physicists and inventors began to work with a new device called a **cathode ray tube**. A cathode ray tube is a glass bulb with the air removed, a hot metal filament at one side, a metallic plate at the other end, and a high voltage between the plate and the

filament. This device simultaneously started the eras of modern quantum physics and modern electronics. Among its many other properties, it was noticed that operating such a cathode ray tube at high voltages had a side effect. The cathode ray tube caused various objects outside of the tube to glow. Although other observers had noticed this effect, it was the german physicist Wilhelm Röntgen (1845-1923) who thought it might be important and undertook a systematic study of the phenomenon.

Röntgen noticed that the glow persisted even when the cathode ray tube was covered up. He called the unknown emissions originating from the cathode ray tube **x-rays**. A name which remains to this day, although they are also known as Röntgen rays in his honor. Moreover, placing a hand between the glow and the tube cast an eerie shadow that illuminated the bones inside his hand in a different light than the surrounding tissue. Röntgen found that this shadow could be photographed. Figure 2 shows one of Röntgen's pictures, one of the earliest x-ray photographs ever taken, dating from 1895. He also found that the x-rays originated in the cathode ray tube at the location where the internal cathode rays struck the metallic plate at the end of the tube. He then established that their degree of penetration through an element depended upon its atomic number. Elements of high atomic number were able to block the x-rays better. Knowing this, he was then able to use slits cut in lead to show that x-rays travel in straight lines and that they are unaffected by electric and magnetic fields. This suggested that the x-rays were a form of electromagnetic radiation similar to light. For his work on x-rays, Röntgen was given the 1901 Nobel prize in physics, the first ever awarded.

Figure 2: An x-ray image of a hand.

If x-rays were similar to light, it seemed reasonable to check whether they exhibit other optical properties of light such as **diffraction**. Diffraction is a wave property of light that makes the edges cast by shadows indistinct instead of sharp and can be used to separate light of different wavelengths. Subsequent investigators had difficulty observing any diffraction and began to suspect that if x-rays were electromagnetic waves like light, they must be of a greatly different wavelength. The German physicist Max von Laue (1879-1960) realized that the spacing of atoms in crystals might be suitable for observing the diffraction of x-rays. His insight was successful and he and his students were the first people to observe **x-ray diffraction** through a crystal. For this work von Laue was awarded the 1914 Nobel prize in physics.

Several more Nobel prizes were earned by physicists studying x-rays. The British son and father team of Sir William L. Bragg (1890-1971) and Sir William H. Bragg (1862-1942) extended von Laue's work. They predicted how x-rays reflect off crystals (a rule now called **Bragg's law** of x-ray diffraction) and used this to design and construct instru-

ments that can examine x-rays by their wavelength. Such instruments are now called **Bragg x-ray spectrometers**. For their work the Bragg's received the 1915 Nobel prize in physics. Further work by the British physicist Charles Barkla (1877-1944) established how x-rays are scattered, polarized, and absorbed. He also discovered that each element emits its own characteristic wavelengths of x-rays which he named **K-shell x-rays**. For this work Barkla received the 1917 Nobel prize in physics. More results on x-ray atomic spectra and still greater refinement of x-ray spectrometers earned the Swedish physicist Karl Siegbahn (1886-1978) a Nobel prize in 1924.

It is now accepted that x-rays are an energetic form of electromagnetic radiation with a much shorter wavelength than light. Ultimately, x-rays became a standard diagnostic tool universally used by astronomers, biologists, chemists, dentists, doctors, engineers, geologists, and physicists. The penetrating nature of x-rays makes it possible to image the interior of living organisms, observe cracks hidden in structures and mechanisms, discern the behaviour of energetic astronomical objects, study the arrangement of atoms in crystals, powders, and alloys, determine the composition of surfaces, and probe the internal energy levels of atomic isotopes.

A point most of these x-ray applications have in common is that they require an x-ray generator, a source of x-rays. Aside from refinements, the **x-ray tubes** used in modern x-ray generators (and the x-ray tube used in this experiment) have the same structure as the original x-ray tubes Röntgen used. Figure 3 shows the structure of an x-ray tube. A hot **cathode** inside an evacuated glass tube emits electrons. These electrons are **accelerated** to the other end of the tube by a high voltage and strike the metal target, called the **anode**. This **electron beam** has enough energy to directly interact with the atoms in the target anode. Most of this energy (about 95%) is lost in the target as heat. The remainder of the energy is converted into x-rays. The target is **bevelled** to give some directionality to the emitted x-rays. Further control of the x-ray beam path is achieved by a lead glass envelope that blocks x-rays in all directions, except for the **aperture** through which the x-rays are permitted to pass.

The x-rays generated by a typical x-ray tube cover a broad range of wavelengths. The proportion of x-rays at any given wavelength is governed by the physical interaction processes between the electrons in the electron beam and the atoms inside the target. A typical spectrum of x-rays emitted by an x-ray tube is shown in Figure 4. It can be seen that the spectrum exhibits two main features. There is a broad curve at all wavelengths to the right of a certain value. Superimposed on this is a set of sharp peaks. It has been found the shape of the smooth part is determined by the magnitude of the high voltage and

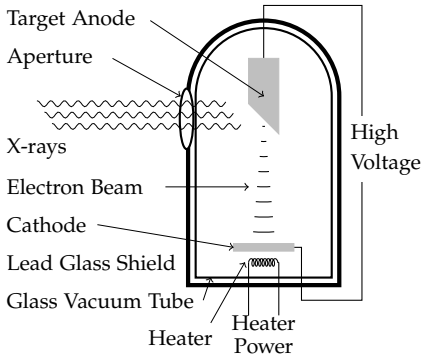

Figure 3: Schematic representation of an x-ray tube.

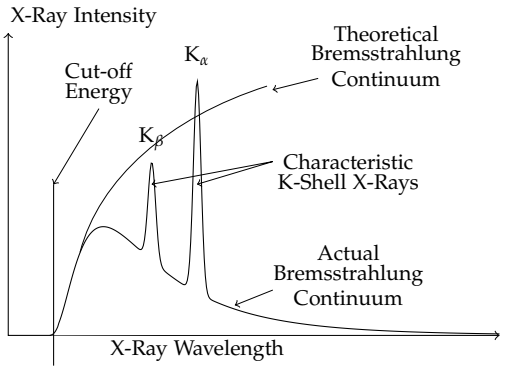

Figure 4: An example of an x-ray spectrum.

the aperture material. The positions and relative sizes of the sharp peaks is determined by the type of atoms the target anode is composed of.

The smooth broad curve is known as the **bremsstrahlung continuum**. This bremsstrahlung radiation, or **braking radiation**, arises due to the acceleration the electrons undergo when they strike the target anode and interact with the electric fields of the atoms inside. Electromagnetic theory predicts that accelerated charges will **radiate** electromagnetic waves. The large number of electrons in the electron beam are all accelerating in different ways since they interact with different atoms of the target at a variety of distances. So the radiated electromagnetic energy happens at many wavelengths and this yields the continuum.

According to the quantum picture, this radiation will be in the form of photons with energy $E = h\nu$ corresponding to the change in the electron kinetic energy Δ K, so that

$$E = h\nu = \Delta K \tag{1}$$

where ν is the frequency of the photon, and $h = 6.62606876 \times 10^{-34}$ Js is **Planck's constant**.

The most energetic possible photon occurs when the electron loses all of its kinetic energy in a single interaction. For an x-ray tube with accelerating voltage, V, the maximum photon energy, E_{max} , and corresponding minimum wavelength λ_{min} is

$$E_{max} = h\nu_{max} = \frac{hc}{\lambda_{min}} = eV \tag{2}$$

where $e = 1.60217646 \times 10^{-19}$ C is the charge of an electron and c = 299792458 m/s is the speed of light. This highest energy is known as the **cut-off energy** of the x-ray tube. An x-ray tube cannot generate x-rays with higher energy than the cut-off energy. At the low end of the spectrum, it seems reasonable to expect that low energy x-rays would be produced in much greater quantities than high energy x-rays near the cut-off. Theoretically, this is indeed correct as can be seen by the theoretical curve shown in Figure 4. However, in practice, it turns out that the low energy x-rays are not detected in great numbers. The reason for this is that low energy x-rays are easily absorbed. The lowest energy x-rays do not even make it out of the target material. Still more are blocked by the glass walls of the x-ray tube, the air, and the entrance walls of the x-ray detector. This results in the characteristic shape of the bremsstrahlung spectrum seen in Figure 4, where numbers of x-rays are small at low energies, increase to some maximum, and then decrease back down to zero at the cut-off.

The other feature of the x-ray tube spectrum is seen to be the sharp

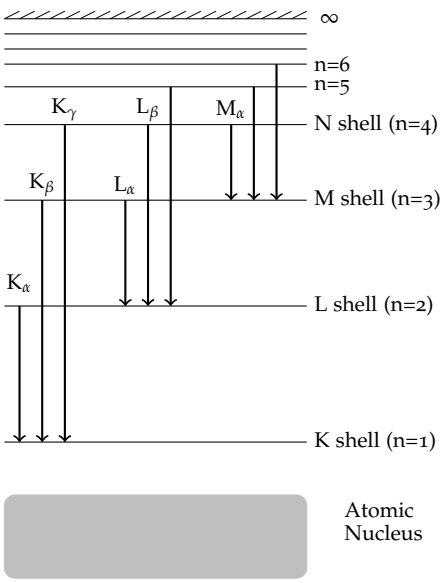

Figure 5: Diagram representing electronic energy levels in an atom.

peaks that rise above the bremsstrahlung continuum. These peaks are also due to interactions between the electrons in the electron beam and the atoms in the target. The energy level model of the atom implies that the electrons surrounding the nucleus of an atom have different energy levels called **shells**. Each electron shell has a designated **principal quantum number**, n. As seen in Figure 5, the innermost shell has quantum number n=1 and is commonly called the **K-shell**. The next shell outward has quantum number n=2 and so on. Any transition of an electron from one level to a lower level must be accompanied by the emission of a photon of energy equal to the energy difference between the two levels.

Electrons in the electron beam of the x-ray tube which are sufficiently energetic can penetrate into the atoms and knock an electron out of an inner shell. In turn, an electron from a higher energy level falls down to fill the hole in the inner shell and thereby releases a photon of the corresponding energy difference. So, for example, when an inner electron from the K-shell is removed from the atom, a common transition is for an electron in the next higher shell (n = 2) to move into the inner shell and emit a photon. As seen in Figure 5, this photon is named K_α. It turns out that for many materials, the K_α photon (and many others) happens to have sufficient energy to be an x-ray photon. Each element has a characteristic set of x-ray peaks corresponding to transitions of electrons between inner energy levels. The height of each peak is related to the probability that the particular electron transition corresponding to that energy difference can happen. These **characteristic x-rays** serve as an identifying marker that can be used to identify the target material and explore its inner atomic energy levels.

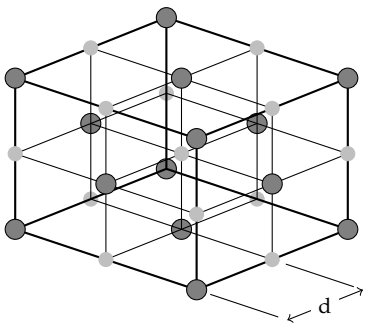

Figure 6: Crystalline structure of a Lithium Fluoride.

It is therefore of strong interest to find a method to determine the wavelengths of the features seen in the x-ray spectrum because the actual wavelengths could be used to measure the energy levels of electronic orbitals inside the atom. What is needed is a device that can separate x-rays by their wavelength. For visible light, the device commonly used for this purpose is called a **diffraction grating**. It consists of a large number of equally spaced parallel lines inscribed onto glass. The spacing of the lines is critical to the operation of the grating. For useable results, the separation between the lines should be roughly the same size or smaller than the wavelength of the light to be diffracted. So for visible light with a wavelength around 500 nm, the spacing of the lines needs to be at least 200 lines per millimeter. Unfortunately, it turns out that the wavelength of x-rays is about 1000 times smaller than the wavelength of visible light. It is quite difficult to machine lines fine enough to serve as a diffraction grating for x-rays. However, the spacing between atoms in a regular solid such as a **crystal** serves very well as a **natural** diffraction grating for x-rays.

This natural correspondence between the x-ray wavelength and the spacing of atoms enables crystals to be used as diffraction gratings for x-rays. The study of crystals and x-rays constitutes the scientific field of **x-ray crystallography**. There is a large abundance of different types of crystals, each with their own structure and properties. This experiment restricts its attention to the simplest type of crystal, an ionic solid with a **cubic structure** as seen in Figure 6. The most common example of this type of solid is ordinary table salt, NaCl. Unfortunately, salt crystals have a tendency to absorb water and break down. For this reason, the cubic ionic crystal used in this experiment instead is **Lithium Fluoride, LiF**. As seen in Figure 5, each atom of lithium is surrounded by six fluorine atoms and conversely, each fluorine atom is surrounded by six lithium atoms. All of the atoms are the same distance from each other and this gives rise to the cubic crystal structure.

It seems reasonable to expect that the spacing between the atoms in the LiF crystal influences how the x-rays diffract through the crystal in the same way that the spacing between ruled lines determines how visible light diffracts through an optical diffraction grating. The cubic structure of LiF makes it possible to calculate the distance between the atoms. Let the **atomic mass** of lithium be denoted by A_{Li} and the atomic mass of fluorine be denoted by A_F. Then the **molar mass**, A_{LiF}, of lithium fluoride is given by

$$A_{LiF} = A_{Li} + A_F \tag{3}$$

The number of molecules in A_{LiF} grams of LiF is N_A, where $N_A = 6.02214199 \times 10^{23}$ is **Avogadro's number**. If the density of LiF is ρ grams per cubic centimeter, then the volume, V, of N_A molecules of LiF must be

$$V = \frac{A_{LiF}}{\rho} \tag{4}$$

cubic centimeters. Since LiF is **diatomic**, the **atomic spacing**, d, in centimeters, between the atoms in LiF is

$$d = \sqrt[3]{\frac{A_{LiF}}{2N_A\rho}} \tag{5}$$

To calculate how the diffraction of x-rays happens inside an LiF crystal, assume that the LiF has a cubic structure and that the x-rays actually are electromagnetic waves. The separation, d, between two neighboring atomic planes is then given by Equation 5. Imagine two x-rays, ray1 and ray2, with wavelength, λ, reflecting off of two planes of atoms inside the crystal with angle of incidence θ as seen in Figure 7. For electromagnetic waves, the angle of reflection equals the angle of incidence, so the reflected ray also leaves the crystal at the same angle

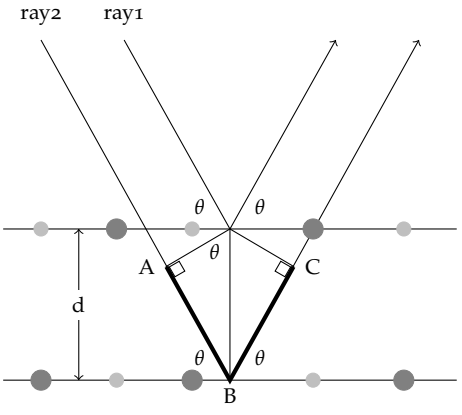

Figure 7: A geometrical perspective on x-ray interaction with a LiF substrate.

θ. If ray1 and ray2 are parallel, then the extra distance travelled by ray2 is the length of the two line segments AB and BC. For **constructive interference** to occur, the distance AB+BC must be an integer multiple of the wavelength. So when x-rays reflect off of the surface of a LiF crystal, each wavelength reflects at a particular angle and all the other wavelengths cancel out. The length of AB is $d \cdot sin(\theta)$, so the condition for constructive interference is

$$n\lambda = 2d\sin(\theta) \quad n = 1, 2, ... \tag{6}$$

This formula is known as **Braggs law** and it describes how x-rays diffract when reflected by a cubic crystal. This diffraction interaction is called **Bragg x-ray diffraction** and it implies that a LiF crystal can be used to measure the wavelength of x-rays simply by tilting it at different angles to the x-ray beam.

The instrument that measures an x-ray spectrum by taking advantage of Bragg's law is called a **Bragg x-ray spectrometer**. The construction of a typical Bragg x-ray spectrometer is shown in Figure 8. An x-ray tube generates a beam of x-rays. The x-ray tube is operated by an

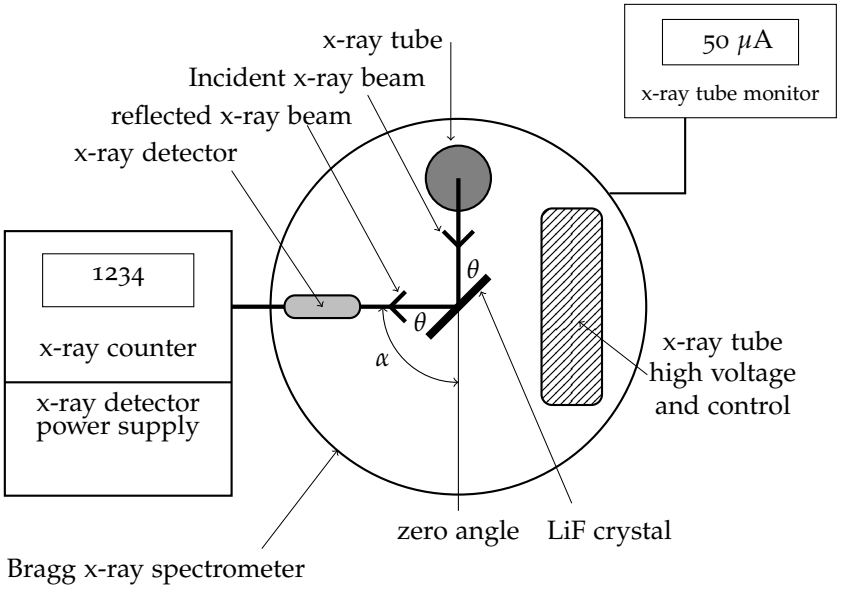

Figure 8: An example of a typical Bragg x-ray spectrometer.

associated high voltage power supply together with control and monitoring electronics. The x-ray beam strikes a mounted crystal at some incident angle θ. Bragg diffraction suggests that the reflected x-rays at the same angle θ will be at the single x-ray wavelength given by Bragg's law, Equation 6. The reflected beam is detected by an **x-ray detector**. An x-ray detector measures the intensity of the reflected

beam. Usually this is done by counting the number of arriving x-ray photons. The x-ray detector also requires its own power supply and control system.

The apparatus is arranged so that the detector can be rotated to any angle α. An internal mechanism links the rotation of the detector to the rotation of the crystal. This is done so that for any detector angle, α, the crystal is positioned such that the angle of incidence, θ, equals the angle of reflection, θ, as seen in Figure 8. The angle α is always twice the angle θ so that

$$\alpha = 2\theta \tag{7}$$

In this way the number of x-rays at any wavelength is determined and when the resulting data is plotted, an x-ray spectrum such as the one in Figure 4 is obtained. The crystal spacing and Equation 6 can then be used to relate an x-ray wavelength to each angle . Equation 6 also suggests that **higher order** spectral features may be visible when $n = 2, 3, \ldots$. In general, higher order spectra are less bright (a smaller number of x-ray photons) than the primary ($n = 1$) spectrum because the extra travel distance through the crystal increases the probablity that the x-ray photon will be absorbed inside the crystal. A more detailed view of the Bragg spectrometer actually used in this experiment is shown in Figure 9. The most significant addition to the instrument are **safety interlocks** and **shielding**. Due to their penetrating nature, x-rays are considered to be harmful radiation when received in

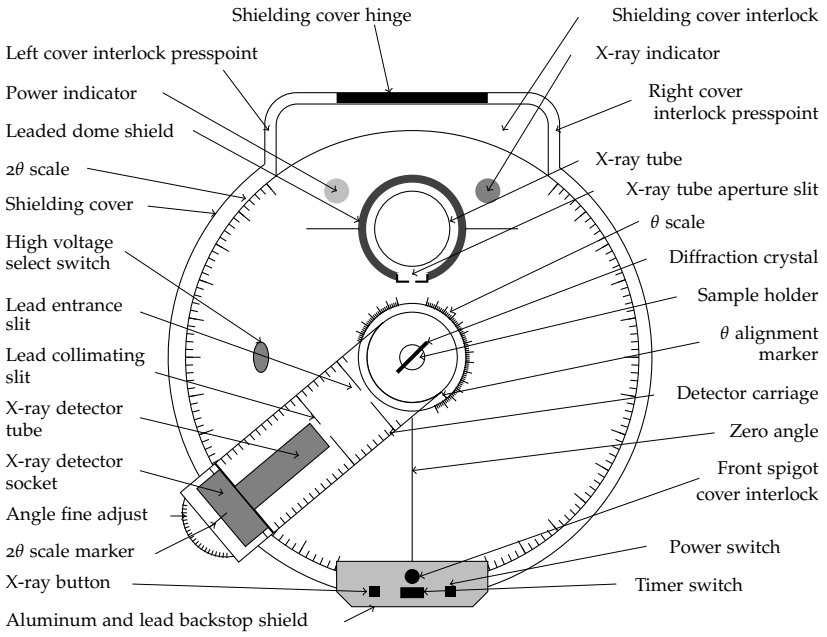

Figure 9: A detailed view of the Bragg spectrometer used in this experiment.

large doses. For this reason, practical x-ray spectrometers are shielded and are equipped with interlocks so that it is impossible to operate the instrument when the shielding is removed. The first layer of shielding is a **dome shield** completely surrounding the x-ray tube and made of leaded glass. An **aperture slit** is mounted in this shield so that a narrow beam of x-rays can escape and strike the diffraction crystal mounted at the center of the x-ray spectrometer. The second layer of shielding are the two lead slits (the **entrance slit** and **collimating slit**) that block the diffracted xrays from escaping the instrument, except for a narrow beam that is permitted to reach the detector. The angular resolution of the x-ray spectrometer is determined by the width of these two slits and the distance between them. The third layer of shielding is the **detector tube** and **detector socket** assembly which absorbs most of the remaining x-rays in the diffracted beam. The fourth layer of shielding is the cover of the instrument. The spectrometer interlocks are designed so that the x-ray tube cannot be energized unless the cover is closed and properly centered. The fifth and final layer of shielding is the **aluminum and lead backstop** that blocks the remaining portion of the direct non-diffracted portion of the x-ray beam. Under normal operation with these safeguards in place, the x-ray spectrometer used in this experiment has been certified as radiologically safe for educational use.

The x-ray spectrometer shown in Figures 8 and 9 can be used to experimentally examine both the production of x-rays by the x-ray tube and the diffraction of x-rays by the sample cystal mounted in the instrument. The x-ray tube used in this experiment has a **copper** target anode. So it is expected that the K-shell peaks visible in the spectrum should originate from copper atoms and have the characteristic energies of copper. The x-ray tube is operated at a voltage of 30 kV and would be expected to produce a bremsstrahlung spectrum with a cut-off as specified by Equation 2 if the theory of braking radiation is correct. The crystal used to diffract the x-rays is lithium fluoride. The density of LiF can be used to deduce the atomic spacing of this crystal assuming a cubic structure. The Bragg spectrometer can then be used to measure the spectrum emitted by the x-ray tube by moving the detector to different angles and recording the x-ray photon count at each angle. If correct, Bragg's law will relate the detector angle to the x-ray wavelength assuming the atomic structure of the crystal is understood. The derived wavelengths of features in the measured x-ray spectrum can be compared with the accepted values to test Bragg's law and the theory of x-ray production and measurement. Lastly, bremsstrahlung can be further examined by placing a thin piece of plastic in the x-ray beam. If the reason for the long low energy tail is actually due to x-ray absorption, then a piece of plastic should attenuate the low energy part

of the spectrum to a much greater extent than the high energy portion. This can be checked by comparing x-ray spectra with and without the plastic against each other.

As is common in spectroscopy, there is a dilemma between accepting the properties of the diffraction grating (in this case a crystal) or accepting the properties of the light source (in this case an x-ray tube). If the grating is trusted, then the grating can be used to measure the spectrum of the incoming x-rays. If the x-ray tube is trusted, then the x-ray beam can be used to examine the atomic structure of the sample being irradiated. In this experiment, neither device is treated as the accepted standard. Instead, the accepted values for the atomic spacing of LiF, the Kα and Kβ wavelengths of copper, and the bremsstrahlung cutoff are compared with the measured values to establish the consistency of the x-ray spectrometer system with x-ray theory. In practice independent evidence is gathered to establish the behaviour of x-ray spectrometers. The structure of LiF is independently deduced by the known chemical properties of ionic solids and the fracture properties of LiF crystals. The wavelengths of x-rays are independently verified without crystals by using ruled gratings that are tilted nearly horizontally to effectively decrease the line spacing of the grating to the point where x-ray diffraction can be obtained.

Experimental Procedure

1. The apparatus is connected together as shown in Figure 8. Make sure all instruments are turned off before proceeding. The x-ray spectrometer is a nearly self-contained unit except for the x-ray counter and the tube current monitor. The x-ray detector cable should be connected to the *GM tube* input connector on the Tel-Atomic Digicounter. The *monitor tube current* output should be connected to the current jacks on the digital multimeter with the supplied cable. Set the multimeter to a range compatible with a current on the order of 50 μA DC.

2. The Tel-Atomic Digicounter powers the x-ray detector tube and accumulates and displays the detected x-ray photon counts. For consistent repeatable operation, that enables comparisons between different instruments, the following settings are recommended. The *GM Tube Supply* voltage should be 420 V. The counting switch should be set to *continuous* and the function switch turned to *radioactivity*. Adjust the range switch to *10s*. Set the timing switch to *stop* and the Triggered setting to *off*. The remaining switches and connections can be neglected.

3. The following checks and configurations are recommended for proper

operation of the x-ray spectrometer. The names of the various spectrometer parts as used here are shown in Figure 9. First lift the spectrometer cover (shielding cover). This cover has an interlock, so there is a special procedure for opening it. As seen in Figure 9, there are cover interlock presspoints on both sides of the spectrometer at the back. To open the cover, press the right interlock presspoint to shift the entire cover left. The cover can be opened once the cover is shifted fully leftwards. The cover hinge is at the rear, so it is opened by reaching under the backstop shield and raising the opening from the front. Once the cover is lifted, examine the instrument. Do **NOT** touch the crystal, it is brittle and sensitive to moisture, but check that it is present, centered in the sample holder, and the top of it has a dab of blue paint. The blue paint identifies the crystal as LiF. Make sure the x-ray tube is installed and fully covered by the lead-glass dome shield. Inspect the backstop shield to make sure there is a thin plate of lead behind the plate of aluminum on the outside of the cover. Set the high voltage select switch to 30 kV. Check that a 1mm lead aperture slit is installed at the exit port of the x-ray tube. Note that the carriage holding the detector has numbered slots. A 1 mm lead collimator should be present in slot 13 of the detector carriage and a 3mm lead collimator should be installed in slot 18. Lastly, the x-ray detector itself should be installed in slot 26 of the detector carriage.

4. Check that the detector carriage moves freely between 12° and 120° on the 2θ scale. For proper operation, the detector carriage must always be on the left side of the instrument as seen in Figures 8 and 9. The reason for this is that the crystal has a preferred face where it has been carefully cleaved, and this is the side that should be exposed to the x-ray beam. Verify that the mechanism which rotates the crystal is working correctly. To do this, rotate the detector and compare the reading on the 2θ scale with the reading on the θ scale. One should be double the other. The 2θ scale is read by the scale marker just behind and underneath the detector socket. The θ scale is read by the angle alignment marker line that is visible on the ring surrounding the sample holder. Next, check the zero alignment of the spectrometer. This is done by rotating the detector to 0° on the 2θ scale. When the zero alignment is correct, the θ scale should also be registering 0° at this point. If there is a mis-alignment, contact the laboratory staff.

5. At this point the instruments are ready to be turned on and the interlocks on the spectrometer checked. Lower the lid and center it using the left and right interlock presspoints. The cover is correctly centered when the front spigot interlock is centered on the the zero

angle line. Check (gently) that the cover cannot be opened when it is centered at this position. Turn on the power to the Digicounter and the multimeter. To power up the spectrometer, rotate the timer switch clockwise to the 50 minute mark and then turn on the power switch. The power indicator should light up and the filament inside the x-ray tube should begin to glow. Then press the x-ray button. If the cover is correctly centered, the x-ray indicator should light up and the spectrometer will begin generating x-rays. If the x-ray indicator does not light, it usually implies that the cover needs a minor position readjustment. Once turned on, check the interlock by pressing the right interlock presspoint and shift the lid left. The x-ray indicator should immediately turn off if the interlocks are operating properly. Re-center the cover and turn the x-rays back on. Report to your laboratory instructor and the laboratory staff if the interlock system is not working correctly.

6. Let the x-ray system warmup and stabilize for about fifteen minutes. Monitor the beam current on the multimeter during this time. The accepted range of operation for the x-ray tube is a beam current between 30 and 70 μA.

7. The spectrometer is now operational. Obtain an x-ray spectrum. At each degree for 2θ between 12° and 120° record the ten second x-ray photon counts. The Digicounter automatically repeats ten second measurements so the reset button on the Digicounter is not required. It is sufficient to make sure that a full ten second measurement is made at each angle before moving the detector onto the next angle. Occasionally check the timer switch, and when it nears zero, again turn the time clockwise back up to 50 minutes. For best results keep the spectrometer running continuously for the entire acquisition of the spectrum.

8. Insert a plastic plate between the two collimators on the detector carriage and obtain a second spectrum in the same manner as the first spectrum.

9. Once the second spectrum is completed, turn off the spectrometer and the other instruments.

Error Analysis

It might be expected that an x-ray spectrum obtained with the Bragg spectrometer used in this experiment would have an appearance something like that shown in Figure 4. This suggests that the x-ray spectra obtained in this experiment are actually graphs of x-ray photon counts versus angle, where the 2θ detector angle is the independent variable

and, N, the number of x-rays, is the dependent variable. As with any graph made from measurements, there will be error bars on each data point reflecting the uncertainty with which it was obtained.

In this experiment, the uncertainty in the angle is dominated by the width of the x-ray beam passing through the instrument. The width of the x-ray beam is determined by the widths and separations of the lead slits in the apparatus. An estimate of the beamwidth can be found by sighting through all of the slits while moving the detector carriage and observing how much the detector must move to each side before the anode of the x-ray tube is blocked. For the instrument used here, it is found that the beamwidth is 3° on the 2θ scale. So the error in 2θ is 1.5° and the error in θ would be at least half of this. Since there are also alignment errors between rotations of the crystal and rotations of the detector, rounding up the error to the nearest degree seems to be prudent. So a reasonable value to use for $u(\theta)$ would be 1°.

Additionally, due to the difficulty in observing angles between the physical lower limit of the spectrometer, 2θ=12°, and the regime of easily measureable angles, $2\theta \geq 17^\circ$, uncertainties in these small-angle measurements should be chosen appropriately.

The detection of x-rays is a statistical process. Each x-ray photon has a particular probability of being counted by the detector. For this reason, the number of x-rays counts varies, even when the angle remains unchanged. If the x-ray count measurement were repeated a large number of times at each angle, a distribution would be obtained, and the width of the distribution would be a good estimate of the error in the x-ray photon count. However, it is known that for photon counters, the distribution typically is gaussian at large count rates and poissonian at small count rates. In either case, a good estimate of the photon count error, $u(N)$, for both of these statistical distributions is

$$u(N) = \sqrt{N} \tag{8}$$

Other sources of systematic error are also present. The precision with which the atomic spacing, d, is known affects the precision with which the x-ray wavelengths can be calculated from Bragg's law. Moreover, the purity, quality, and uniformity of the crystal are large factors in the sharpness of the observed features in the x-ray spectrum. If the spacing of the LiF atoms is not identically cubic due to impurities or imperfections, then the analysis of Bragg x-ray diffraction as presented here does not fully apply. Lastly, the photons counted by the x-ray detector do not all arrive from the x-ray beam. Other radioactive sources such as cosmic rays and trace amounts of isotopes in the spectrometer and surroundings contribute as well. These extra sources of photons are called background radiation. For this experiment, errors in the crystal lattice spacing and background radiation can be neglected.

To be handed in to your laboratory instructor.

Prelab

1. The x-ray region of the electromagnetic spectrum extends between the frequencies of 10^{17} Hz and 10^{20} Hz. For x-rays of these two frequencies, calculate the corresponding wavelength in nanometers and the corresponding energy in keV.

2. Find the energy, in keV, of an electron accelerated across a 30kV potential difference. What is the cut-off energy, in keV, of a 30kV x-ray tube?

3. In Figure 4, explain whether it is the left side or the right side of the x-ray spectrum that is the high energy side.

4. Look up the atomic masses of lithium and fluorine, and the density of LiF. Using these values calculate the atomic spacing of LiF.

5. Look up the K-shell characteristic x-ray energies for copper.

Data Requirements

6. A data table of the x-ray spectrum together with appropriate errors.

7. A data table, with errors, of the x-ray spectrum with the plastic plate inserted into the beam.

8. A graph of counts versus angle θ with error bars for both x-ray spectra.

9. A graph of counts versus wavelength in nanometers with error bars for both x-ray spectra.

10. A graph of counts versus energy in keV with error bars for both x-ray spectra.

11. A value, with error, for the estimated cut-off wavelength, λ_{min}, of the of the x-ray tube.

12. A value, with error, for Planck's constant as derived from the cut-off wavelength.

13. Values, with error, for the observed K-shell characteristic x-rays of copper.

Discussion

14. A comparison of the observed x-ray spectrum with the expected spectrum.

15. A comparison of the observed x-ray spectrum with the observed x-ray spectrum with the plastic inserted.

16. A comparison of the observed cut-off and derived Planck's constant with the expected values.

17. A comparison of the K-shell characteristic x-rays of copper with the accepted values.

18. Discuss whether your results support or refute the hypothesis that x-rays are electromagnetic waves produced in the copper target of the x-ray tube by bremsstrahlung and K-shell interactions and diffracted by the LiF crystal.

19. Using your results, explain why the third and fourth (if visible) peaks are more more likely to be n=2 versions of the first two peaks rather than separate characteristic x-rays.

20. The method of tilting a grating at an extreme angle to effectively get a very small spacing between lines is called the **grazing incidence technique**. Figure 10 shows a tilted grating with distance AB between adjacent grooves. Calculate the angle θ required so that the effective grating spacing BC is 1/1000th the spacing of AB.

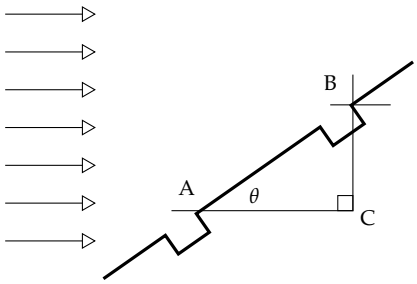

Figure 10: A schematic representation of the grazing incidence technique.

X-Ray Diffraction - Companion Guide

Equipment

- Tel-X-ometer x-ray spectrometer
- LiF crystal diffraction grating
- Geiger counter detector
- 1mm and 3mm lead collimator slides
- Tel-Atomic Digicounter digital pulse counter
- X-ray tube current monitoring cable
- Fluke multimeter
- Acrylic plastic x-ray attenuator slide plate

Setup

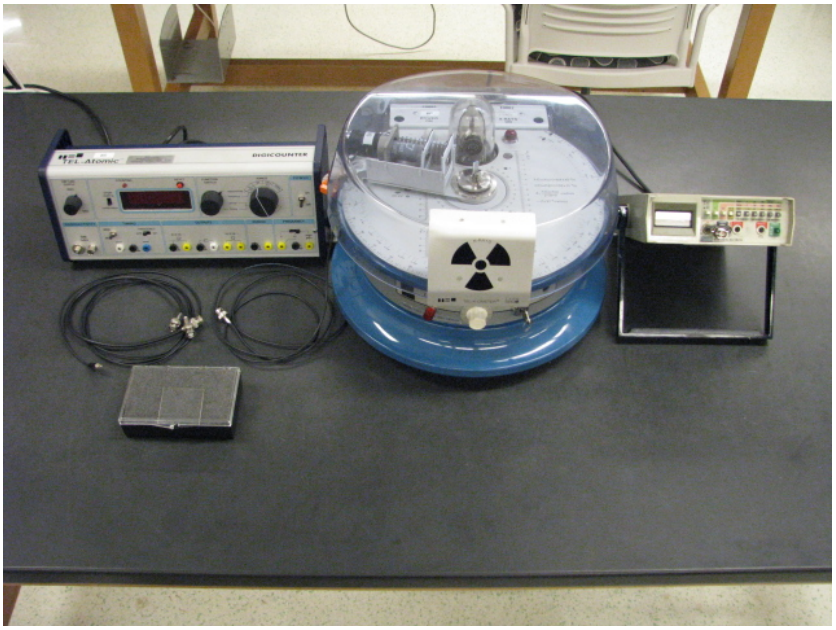

Figure 11: Equipment Setup

Set up bench as shown in Figure 11.

Maintenance

1.

2.

Critical Points of Failure

There are currently no known critical points of failure.

Notes to the Instructor

1. It is practical to take standard single-degree steps when measuring the bremsstrahlung continuum however it is recommended that students take smaller, half-degree steps around the characteristic peaks to improve the resolution of their spectra.

Prelab Questions

1. **The x-ray region of the electromagnetic spectrum extends between the frequencies of 10^{17} Hz and 10^{20} Hz. For x-rays of these two frequencies, calculate the corresponding wavelength in nanometers and the corresponding energy in keV.**

   We know that $c = \lambda\nu$ and that E=hν. Using these relationships we can find that 10^{17} Hz=3 nm=0.4136 keV and 10^{20} Hz=0.003 nm=413.6 keV.

2. **Find the energy, in keV, of an electron accelerated across a 30kV potential difference. What is the cut-off energy, in keV, of a 30kV x-ray tube?**

   1 keV is the energy gained by a single electron crossing a potential difference of 1 V. In this case, the electron will gain 30 keV of energy. If we have a 30 keV x-ray tube, we should see no photons possessing higher energy than 30 keV, thus 30 keV would be the cut-off energy.

3. **In Figure 4, explain whether it is the left side or the right side of the x-ray spectrum that is the high energy side.**

   Using the following relationship,

$$n\lambda = 2dsin\theta \tag{9}$$

We can see that λ is maximal when $\theta = 90^\circ$ and minimal when $\theta = 0^\circ$. This means that the left side of the plot, i.e., the smaller angles, correspond to shorter wavelengths and higher energies and the right side of the plot, i.e., the larger angles, correspond to longer wavelengths and lower energies.

4. **Look up the atomic masses of lithium and fluorine, and the density of LiF. Using these values calculate the atomic spacing of LiF.**

   A_{Li}=6.94 g mol^{-1} and A_F=19.0 g mol^{-1} so A_{LiF}=25.94 g mol^{-1}. The density of LiF, ρ, is 2.64 g cm^{-3}. We use the following relation to find the interatomic spacing of LiF,

$$d = \sqrt[3]{\frac{A_{LiF}}{2N_A\rho}} = \sqrt[3]{\frac{25.94}{2(6.022 \times 10^{23})(2.64)}} = 0.2013nm \qquad (10)$$

5. **Look up the K-shell characteristic x-ray energies for copper.**

   K-shell characteristic energies for copper are $K_\alpha = 8.038$ keV and $K_\beta = 8.905$ keV[1]. These are first order lines. With the LiF crystal used in this lab, students will also see second order lines.

[1] http://www.phywe-es.com/index.php/fuseaction/download/lrn_file/versuchsanleitungen/P2540101/e/P2540101E.pdf

Data Requirements

1. **A data table of the x-ray spectrum together with appropriate errors.**

   See Tables 1-3.

2. **A data table, with errors, of the x-ray spectrum with the plastic plate inserted into the beam.**

   See Tables 4-5.

3. **A graph of counts versus angle θ with error bars for both x-ray spectra.**

   See Figure 12.

4. **A graph of counts versus wavelength in nanometers with error bars for both x-ray spectra.**

   See Figure 13.

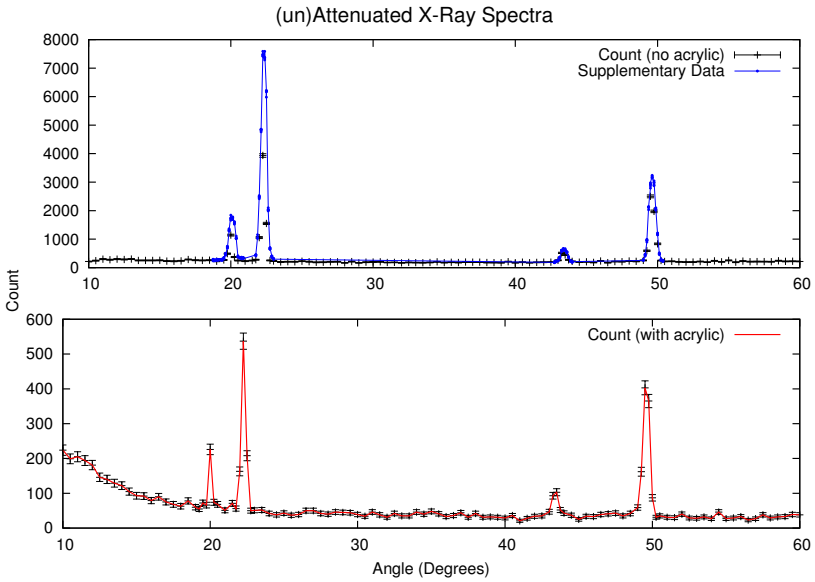

Figure 12: The top plot includes higher angular resolution data (in blue) to illustrate more clearly the location of the peaks. Additionally, multiple sets of counts were collected for each high resolution angle to verify that the variance in measurements was at least Poissonian. The bottom plot shows the data obtained for measurements of every degree with the acrylic slide in place. Uncertainties in the angle measurements are not included here to keep the plots uncluttered.

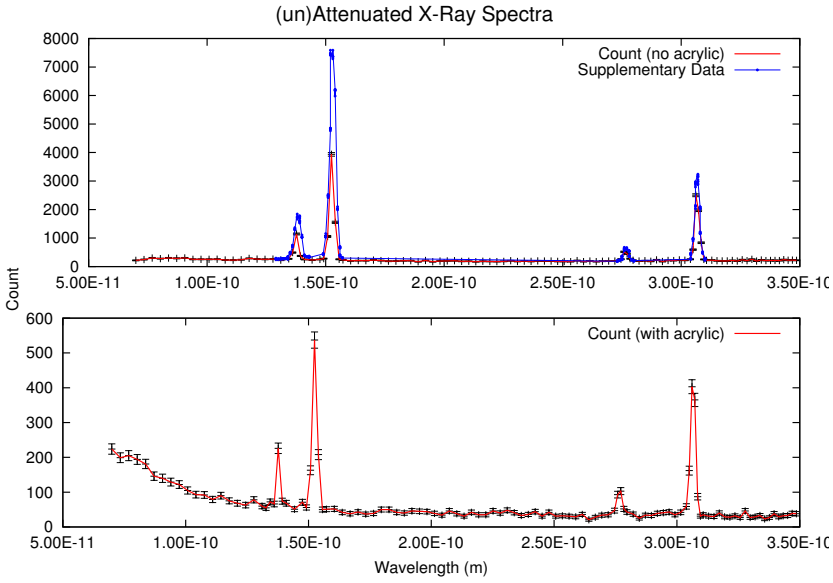

Figure 13: This plot shows the wavelength (m) of the characteristic peaks of copper with and without the acrylic slide. Supplementary data is in blue.

5. **A graph of counts versus energy in keV with error bars for both x-ray spectra.**

   See Figure 14.

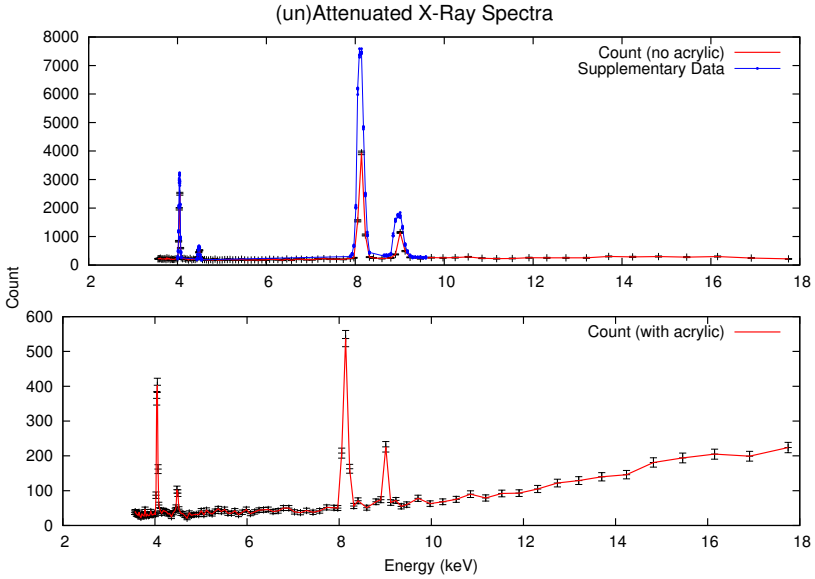

Figure 14: This plot shows the energies (keV) of the characteristic peaks of copper with and without the acrylic slide. Supplementary data is in blue. The cut-off energy cannot be seen due to the physical constraints of the equipment.

6. **A value, with error, for the estimated cut-off wavelength, λ_{min}, of the of the x-ray tube.**

   Depending on the condition of the Bragg spectrometer that students use there may be varying degrees of success in obtaining a satisfactory data set for determining the cut-off energy. Ideally, students will obtain a spectrum such as that shown in Figure 15 from which they can discern the cut-off angle and thus the cut-off energy. It is likely that many won't however and so it is necessary to record appropriate magnitudes of uncertainty in extrapolations of the graph.

   Using the data from Figure 15 we estimate the cut-off angle to be $6\pm1^\circ$. This corresponds to a wavelength of 42.1 ± 6.99 picometers

7. **A value, with error, for Planck's constant as derived from the cut-off wavelength.**

   The Planck constant can be calculated as follows,

$$h = \frac{eV}{c} \cdot 2d \cdot sin(\theta_{min}) = 4.208 \times 10^{-15} \tag{11}$$

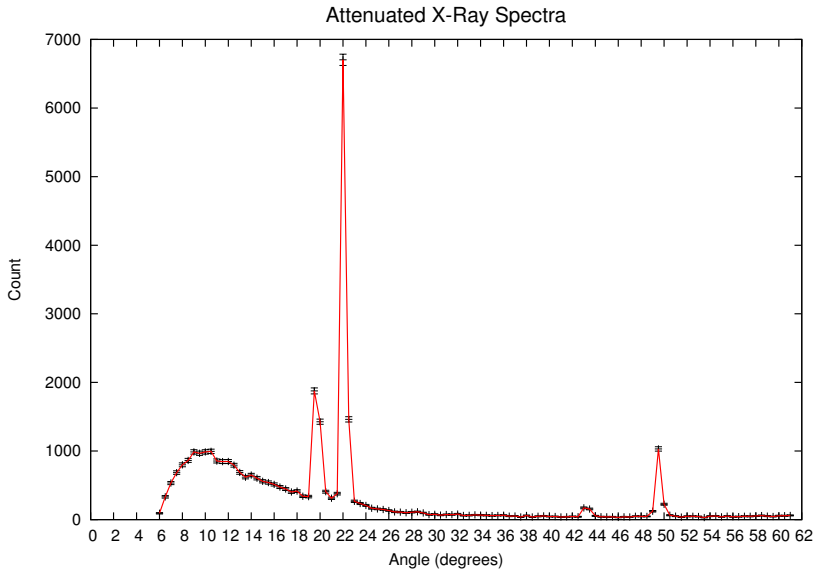

Figure 15: Ideal spectrum for experimentally determining the cut-off energy of the Bragg x-ray spectrometer. Here the cut-off angle is easily extrapolated from the plot.

Where eV is 30 keV corresponding to the spectrometer's energy setting and θ_{min} is the value extrapolated from the graph. The uncertainty is found from

$$u(h) = \frac{eV}{c} \cdot 2d \cdot cos(\theta_{min}) \cdot u(\theta_{min}) = 6.988 \times 10^{-16} \qquad (12)$$

8. **Values, with error, for the observed K-shell characteristic x-rays of copper.**

The two values desired here are for K_α and K_β. K_α is actually a doublet but it is beyond the ability of this spectrometer to resolve it so we take the average value of the doublet to be E=8.038 keV. The energy of K_β is taken to be E=8.905 keV.

Reading from our data (see Tables 1-3 we see that the highest counts are obtained at energies of 8.139$\pm$ 0.174 keV and 9.010$\pm$0.216 keV. This gives us percent errors of 1.26% for the K_α line and 1.18% for the K_β line. These values are well within experimental uncertainty. Accepted values for the characteristic energies of copper can be found in the Handbook of Chemistry and Physics, CRC Press, available online.

Discussion

9. **A comparison of the observed x-ray spectrum with the expected spectrum.**

In our spectrum we see evidence of the expected braking radiation, smoothly spread across all energies and ending at the cut-off energy of the spectrometer. We also see the first and second order characteristic spikes of copper at the expected energies. We do not, however, see the K_α doublet. This is likely beyond the resolution of the spectrometer because of its relatively large beam width.

10. **A comparison of the observed x-ray spectrum with the observed x-ray spectrum with the plastic inserted.**

We again see the characteristic energy spikes of copper in their expected positions. Regarding the braking radiation, the right-skewed shape is more prominent when we attenuate the lower energy x-rays with the acrylic slide. This makes it somewhat easier to extrapolate the curve towards the cut-off energy (see Figure 15).

11. **A comparison of the observed cut-off and derived Planck's constant with the expected values.**

Experimentally determined values for the cut-off energy (29.482 ± 4.896 keV) and the Planck constant ($4.208 \times 10^{-15} \pm 6.988 \times 10^{-16}$ eV s) agreed with literature values (30 keV and 4.136×10^{-15} eV s, respectively) to within uncertainty.

12. **A comparison of the K-shell characteristic x-rays of copper with the accepted values.**

Reading from our data (see Tables 1-3 we see that the highest counts are obtained at energies of 8.139 ± 0.174 keV and 9.010 ± 0.216 keV. This gives us percent errors of 1.26% for the K_α line and 1.18% for the K_β line. These values are well within experimental uncertainty. Accepted values for the characteristic energies of copper can be found in the CRC Handbook, available online.

13. **Discuss whether your results support or refute the hypothesis that x-rays are electromagnetic waves produced in the copper target of the x-ray tube by bremsstrahlung and K-shell interactions and diffracted by the LiF crystal.**

All the predictions made under the assumption of the correctness of electromagnetic and spectroscopic theory as presented in this lab are supported by our results to within experimental uncertainties.

14. **Using your results, explain why the third and fourth (if visible) peaks are more more likely to be n=2 versions of the first two peaks rather than separate characteristic x-rays.**

Because the K_β line is only ~73 keV away from the ionization energy for copper we would expect that any higher energy lines would need to be very tightly packed and immediately following the K_β line and at lower angles, i.e., higher energy. This is not what we see from the second set of lines in our spectra. These lines are at higher angles and lower energy. Given that the K_α line is predicted to be a transition from n=2 to n=1 we would expect no characteristic lines to be found at lower energies than K_α. This leaves one possibility; the additional lines seen are the result of higher order diffraction.

15. **The method of tilting a grating at an extreme angle to effectively get a very small spacing between lines is called the grazing incidence technique. Figure 10 shows a tilted grating with distance AB between adjacent grooves. Calculate the angle θ required so that the effective grating spacing BC is 1/1000th the spacing of AB.**

The effective spacing, d_{eff}, is given by,

$$d_{eff} = dsin(\theta) \tag{13}$$

We want d_{eff} to be d/1000.

$$\frac{d}{1000} = dsin(\theta) \tag{14}$$

$$\theta = sin^{-1}\left(\frac{1}{1000}\right) = 0.057^\circ \tag{15}$$

So the minimum angle necessary to achieve a line spacing that is $1/1000^{th}$ of the original, AB, is 0.057°.

2θ	u(2θ)	θ	u(θ)	Count	u(Count)	λ (m)	u(λ) (m)	Energy (keV)	u(Energy) (keV)
20	1.0	10	0.5	217	14.7	6.99E-11	3.46E-12	17.7469	0.8783
21	1.0	10.5	0.5	247	15.7	7.34E-11	3.45E-12	16.9106	0.7962
22	1.0	11	0.5	300	17.3	7.68E-11	3.45E-12	16.1508	0.7251
23	1.0	11.5	0.5	279	16.7	8.03E-11	3.44E-12	15.4574	0.6630
24	1.0	12	0.5	300	17.3	8.37E-11	3.44E-12	14.8223	0.6085
25	1.0	12.5	0.5	288	17.0	8.71E-11	3.43E-12	14.2382	0.5605
26	1.0	13	0.5	303	17.4	9.06E-11	3.42E-12	13.6995	0.5178
27	1.0	13.5	0.5	256	16.0	9.40E-11	3.42E-12	13.2010	0.4798
28	1.0	14	0.5	253	15.9	9.74E-11	3.41E-12	12.7385	0.4459
29	1.0	14.5	0.5	255	16.0	1.01E-10	3.40E-12	12.3082	0.4153
30	1.0	15	0.5	257	16.0	1.04E-10	3.39E-12	11.9069	0.3878
31	1.0	15.5	0.5	232	15.2	1.08E-10	3.39E-12	11.5317	0.3629
32	1.0	16	0.5	227	15.1	1.11E-10	3.38E-12	11.1803	0.3403
33	1.0	16.5	0.5	240	15.5	1.14E-10	3.37E-12	10.8505	0.3197
34	1.0	17	0.5	286	16.9	1.18E-10	3.36E-12	10.5404	0.3009
35	1.0	17.5	0.5	261	16.2	1.21E-10	3.35E-12	10.2483	0.2836
36	1.0	18	0.5	256	16.0	1.24E-10	3.34E-12	9.9727	0.2678
37	1.0	18.5	0.5	263	16.2	1.28E-10	3.33E-12	9.7122	0.2533
38	1.0	19	0.5	225	15.0	1.31E-10	3.32E-12	9.4657	0.2399
39	1.0	19.5	0.5	269	16.4	1.34E-10	3.31E-12	9.2320	0.2275
39.5	1.0	19.75	0.5	491	22.2	1.36E-10	3.31E-12	9.1198	0.2217
40	1.0	20	0.5	1143	33.8	1.38E-10	3.30E-12	9.0103	0.2160
40.5	1.0	20.25	0.5	373	19.3	1.39E-10	3.30E-12	8.9037	0.2106
41	1.0	20.5	0.5	250	15.8	1.41E-10	3.29E-12	8.7997	0.2054
42	1.0	21	0.5	231	15.2	1.44E-10	3.28E-12	8.5993	0.1955
43	1.0	21.5	0.5	249	15.8	1.48E-10	3.27E-12	8.4085	0.1863
43.5	1.0	21.75	0.5	280	16.7	1.49E-10	3.26E-12	8.3164	0.1819
44	1.0	22	0.5	1056	32.5	1.51E-10	3.26E-12	8.2265	0.1777
44.5	1.0	22.25	0.5	3936	62.7	1.52E-10	3.25E-12	8.1387	0.1736
45	1.0	22.5	0.5	1552	39.4	1.54E-10	3.25E-12	8.0529	0.1697
45.5	1.0	22.75	0.5	253	15.9	1.56E-10	3.24E-12	7.9691	0.1658
46	1.0	23	0.5	235	15.3	1.57E-10	3.23E-12	7.8871	0.1621
47	1.0	23.5	0.5	200	14.1	1.61E-10	3.22E-12	7.7285	0.1551
48	1.0	24	0.5	209	14.5	1.64E-10	3.21E-12	7.5767	0.1485
49	1.0	24.5	0.5	207	14.4	1.67E-10	3.20E-12	7.4313	0.1423
50	1.0	25	0.5	228	15.1	1.70E-10	3.18E-12	7.2920	0.1365
51	1.0	25.5	0.5	210	14.5	1.73E-10	3.17E-12	7.1583	0.1310
52	1.0	26	0.5	189	13.7	1.76E-10	3.16E-12	7.0299	0.1258
53	1.0	26.5	0.5	191	13.8	1.80E-10	3.14E-12	6.9066	0.1209
54	1.0	27	0.5	204	14.3	1.83E-10	3.13E-12	6.7881	0.1163
55	1.0	27.5	0.5	207	14.4	1.86E-10	3.12E-12	6.6740	0.1119
56	1.0	28	0.5	170	13.0	1.89E-10	3.10E-12	6.5642	0.1077
57	1.0	28.5	0.5	214	14.6	1.92E-10	3.09E-12	6.4585	0.1038
58	1.0	29	0.5	170	13.0	1.95E-10	3.07E-12	6.3566	0.1001
59	1.0	29.5	0.5	193	13.9	1.98E-10	3.06E-12	6.2583	0.0965
60	1.0	30	0.5	199	14.1	2.01E-10	3.04E-12	6.1634	0.0932

Table 1: Data for unattenuated x-rays.

2θ	u(2θ)	θ	u(θ)	Count	u(Count)	λ (m)	u(λ) (m)	Energy (keV)	u(Energy) (keV)
61	1.0	30.5	0.5	204	14.3	2.04E-10	3.03E-12	6.0719	0.0900
62	1.0	31	0.5	182	13.5	2.07E-10	3.01E-12	5.9835	0.0869
63	1.0	31.5	0.5	186	13.6	2.10E-10	3.00E-12	5.8980	0.0840
64	1.0	32	0.5	170	13.0	2.13E-10	2.98E-12	5.8155	0.0812
65	1.0	32.5	0.5	184	13.6	2.16E-10	2.96E-12	5.7356	0.0786
66	1.0	33	0.5	178	13.3	2.19E-10	2.95E-12	5.6583	0.0760
67	1.0	33.5	0.5	173	13.2	2.22E-10	2.93E-12	5.5835	0.0736
68	1.0	34	0.5	183	13.5	2.25E-10	2.91E-12	5.5110	0.0713
69	1.0	34.5	0.5	205	14.3	2.28E-10	2.90E-12	5.4408	0.0691
70	1.0	35	0.5	178	13.3	2.31E-10	2.88E-12	5.3728	0.0670
71	1.0	35.5	0.5	190	13.8	2.34E-10	2.86E-12	5.3069	0.0649
72	1.0	36	0.5	180	13.4	2.37E-10	2.84E-12	5.2429	0.0630
73	1.0	36.5	0.5	198	14.1	2.39E-10	2.82E-12	5.1809	0.0611
74	1.0	37	0.5	195	14.0	2.42E-10	2.81E-12	5.1207	0.0593
75	1.0	37.5	0.5	194	13.9	2.45E-10	2.79E-12	5.0623	0.0576
76	1.0	38	0.5	181	13.5	2.48E-10	2.77E-12	5.0055	0.0559
77	1.0	38.5	0.5	179	13.4	2.51E-10	2.75E-12	4.9504	0.0543
78	1.0	39	0.5	175	13.2	2.53E-10	2.73E-12	4.8969	0.0528
79	1.0	39.5	0.5	212	14.6	2.56E-10	2.71E-12	4.8449	0.0513
80	1.0	40	0.5	175	13.2	2.59E-10	2.69E-12	4.7943	0.0499
81	1.0	40.5	0.5	193	13.9	2.61E-10	2.67E-12	4.7451	0.0485
82	1.0	41	0.5	173	13.2	2.64E-10	2.65E-12	4.6973	0.0472
83	1.0	41.5	0.5	187	13.7	2.67E-10	2.63E-12	4.6508	0.0459
84	1.0	42	0.5	193	13.9	2.69E-10	2.61E-12	4.6056	0.0446
85	1.0	42.5	0.5	195	14.0	2.72E-10	2.59E-12	4.5615	0.0434
86	1.0	43	0.5	258	16.1	2.75E-10	2.57E-12	4.5187	0.0423
86.5	1.0	43.25	0.5	518	22.8	2.76E-10	2.56E-12	4.4977	0.0417
87	1.0	43.5	0.5	449	21.2	2.77E-10	2.55E-12	4.4769	0.0412
87.5	1.0	43.75	0.5	273	16.5	2.78E-10	2.54E-12	4.4565	0.0406
88	1.0	44	0.5	221	14.9	2.80E-10	2.53E-12	4.4363	0.0401
89	1.0	44.5	0.5	194	13.9	2.82E-10	2.51E-12	4.3967	0.0390
90	1.0	45	0.5	204	14.3	2.85E-10	2.48E-12	4.3582	0.0380
91	1.0	45.5	0.5	185	13.6	2.87E-10	2.46E-12	4.3207	0.0371
92	1.0	46	0.5	235	15.3	2.90E-10	2.44E-12	4.2841	0.0361
93	1.0	46.5	0.5	176	13.3	2.92E-10	2.42E-12	4.2485	0.0352
94	1.0	47	0.5	215	14.7	2.94E-10	2.40E-12	4.2137	0.0343
95	1.0	47.5	0.5	211	14.5	2.97E-10	2.37E-12	4.1799	0.0334
96	1.0	48	0.5	233	15.3	2.99E-10	2.35E-12	4.1469	0.0326
97	1.0	48.5	0.5	222	14.9	3.02E-10	2.33E-12	4.1147	0.0318
98	1.0	49	0.5	255	16.0	3.04E-10	2.30E-12	4.0833	0.0310
98.5	1.0	49.25	0.5	592	24.3	3.05E-10	2.29E-12	4.0679	0.0306
99	1.0	49.5	0.5	2502	50.0	3.06E-10	2.28E-12	4.0527	0.0302
99.5	1.0	49.75	0.5	1975	44.4	3.07E-10	2.27E-12	4.0377	0.0298
100	1.0	50	0.5	837	28.9	3.08E-10	2.26E-12	4.0229	0.0295
100.5	1.0	50.25	0.5	252	15.9	3.10E-10	2.25E-12	4.0083	0.0291

Table 2: Data for unattenuated x-rays.

2θ	u(2θ)	θ	u(θ)	Count	u(Count)	λ (m)	u(λ) (m)	Energy (keV)	u(Energy) (keV)
101	1.0	50.5	0.5	219	14.8	3.11E-10	2.23E-12	3.9938	0.0287
102	1.0	51	0.5	224	15.0	3.13E-10	2.21E-12	3.9654	0.0280
103	1.0	51.5	0.5	205	14.3	3.15E-10	2.19E-12	3.9378	0.0273
104	1.0	52	0.5	196	14.0	3.17E-10	2.16E-12	3.9108	0.0267
105	1.0	52.5	0.5	196	14.0	3.19E-10	2.14E-12	3.8844	0.0260
106	1.0	53	0.5	216	14.7	3.22E-10	2.11E-12	3.8587	0.0254
107	1.0	53.5	0.5	194	13.9	3.24E-10	2.09E-12	3.8337	0.0248
108	1.0	54	0.5	238	15.4	3.26E-10	2.07E-12	3.8092	0.0242
109	1.0	54.5	0.5	204	14.3	3.28E-10	2.04E-12	3.7854	0.0236
110	1.0	55	0.5	255	16.0	3.30E-10	2.02E-12	3.7621	0.0230
111	1.0	55.5	0.5	193	13.9	3.32E-10	1.99E-12	3.7394	0.0224
112	1.0	56	0.5	231	15.2	3.34E-10	1.96E-12	3.7172	0.0219
113	1.0	56.5	0.5	212	14.6	3.36E-10	1.94E-12	3.6956	0.0213
114	1.0	57	0.5	214	14.6	3.38E-10	1.91E-12	3.6745	0.0208
115	1.0	57.5	0.5	213	14.6	3.40E-10	1.89E-12	3.6540	0.0203
116	1.0	58	0.5	208	14.4	3.41E-10	1.86E-12	3.6339	0.0198
117	1.0	58.5	0.5	243	15.6	3.43E-10	1.84E-12	3.6143	0.0193
118	1.0	59	0.5	221	14.9	3.45E-10	1.81E-12	3.5952	0.0189
119	1.0	59.5	0.5	225	15.0	3.47E-10	1.78E-12	3.5766	0.0184
120	1.0	60	0.5	219	14.8	3.49E-10	1.76E-12	3.5585	0.0179

Table 3: Data for unattenuated x-rays.

2θ	u(2θ)	θ	u(θ)	Count	u(Count)	λ (m)	u(λ) (m)	Energy (keV)	u(Energy) (keV)
20	1.0	10	0.5	224	15.0	6.99E-11	3.46E-12	17.7469	0.8783
21	1.0	10.5	0.5	199	14.1	7.34E-11	3.45E-12	16.9106	0.7962
22	1.0	11	0.5	205	14.3	7.68E-11	3.45E-12	16.1508	0.7251
23	1.0	11.5	0.5	194	13.9	8.03E-11	3.44E-12	15.4574	0.6630
24	1.0	12	0.5	181	13.5	8.37E-11	3.44E-12	14.8223	0.6085
25	1.0	12.5	0.5	146	12.1	8.71E-11	3.43E-12	14.2382	0.5605
26	1.0	13	0.5	140	11.8	9.06E-11	3.42E-12	13.6995	0.5178
27	1.0	13.5	0.5	129	11.4	9.40E-11	3.42E-12	13.2010	0.4798
28	1.0	14	0.5	122	11.0	9.74E-11	3.41E-12	12.7385	0.4459
29	1.0	14.5	0.5	105	10.2	1.01E-10	3.40E-12	12.3082	0.4153
30	1.0	15	0.5	93	9.6	1.04E-10	3.39E-12	11.9069	0.3878
31	1.0	15.5	0.5	92	9.6	1.08E-10	3.39E-12	11.5317	0.3629
32	1.0	16	0.5	79	8.9	1.11E-10	3.38E-12	11.1803	0.3403
33	1.0	16.5	0.5	90	9.5	1.14E-10	3.37E-12	10.8505	0.3197
34	1.0	17	0.5	75	8.7	1.18E-10	3.36E-12	10.5404	0.3009
35	1.0	17.5	0.5	68	8.2	1.21E-10	3.35E-12	10.2483	0.2836
36	1.0	18	0.5	63	7.9	1.24E-10	3.34E-12	9.9727	0.2678
37	1.0	18.5	0.5	78	8.8	1.28E-10	3.33E-12	9.7122	0.2533
38	1.0	19	0.5	60	7.7	1.31E-10	3.32E-12	9.4657	0.2399
38.5	1.0	19.25	0.5	55	7.4	1.33E-10	3.32E-12	9.3473	0.2336
39	1.0	19.5	0.5	72	8.5	1.34E-10	3.31E-12	9.2320	0.2275
39.5	1.0	19.75	0.5	66	8.1	1.36E-10	3.31E-12	9.1198	0.2217
40	1.0	20	0.5	226	15.0	1.38E-10	3.30E-12	9.0103	0.2160
40.5	1.0	20.25	0.5	74	8.6	1.39E-10	3.30E-12	8.9037	0.2106
41	1.0	20.5	0.5	68	8.2	1.41E-10	3.29E-12	8.7997	0.2054
42	1.0	21	0.5	51	7.1	1.44E-10	3.28E-12	8.5993	0.1955
43	1.0	21.5	0.5	71	8.4	1.48E-10	3.27E-12	8.4085	0.1863
43.5	1.0	21.75	0.5	56	7.5	1.49E-10	3.26E-12	8.3164	0.1819
44	1.0	22	0.5	163	12.8	1.51E-10	3.26E-12	8.2265	0.1777
44.5	1.0	22.25	0.5	537	23.2	1.52E-10	3.25E-12	8.1387	0.1736
45	1.0	22.5	0.5	208	14.4	1.54E-10	3.25E-12	8.0529	0.1697
45.5	1.0	22.75	0.5	50	7.1	1.56E-10	3.24E-12	7.9691	0.1658
46	1.0	23	0.5	51	7.1	1.57E-10	3.23E-12	7.8871	0.1621
47	1.0	23.5	0.5	52	7.2	1.61E-10	3.22E-12	7.7285	0.1551
48	1.0	24	0.5	42	6.5	1.64E-10	3.21E-12	7.5767	0.1485
49	1.0	24.5	0.5	38	6.2	1.67E-10	3.20E-12	7.4313	0.1423
50	1.0	25	0.5	43	6.6	1.70E-10	3.18E-12	7.2920	0.1365
51	1.0	25.5	0.5	37	6.1	1.73E-10	3.17E-12	7.1583	0.1310
52	1.0	26	0.5	39	6.2	1.76E-10	3.16E-12	7.0299	0.1258
53	1.0	26.5	0.5	50	7.1	1.80E-10	3.14E-12	6.9066	0.1209
54	1.0	27	0.5	50	7.1	1.83E-10	3.13E-12	6.7881	0.1163
55	1.0	27.5	0.5	42	6.5	1.86E-10	3.12E-12	6.6740	0.1119

Table 4: Data for x-rays attenuated by an acrylic slide.

2θ	u(2θ)	θ	u(θ)	Count	u(Count)	λ (m)	u(λ) (m)	Energy (keV)	u(Energy) (keV)
56	1.0	28	0.5	40	6.3	1.89E-10	3.10E-12	6.5642	0.1077
57	1.0	28.5	0.5	46	6.8	1.92E-10	3.09E-12	6.4585	0.1038
58	1.0	29	0.5	45	6.7	1.95E-10	3.07E-12	6.3566	0.1001
59	1.0	29.5	0.5	44	6.6	1.98E-10	3.06E-12	6.2583	0.0965
60	1.0	30	0.5	39	6.2	2.01E-10	3.04E-12	6.1634	0.0932
61	1.0	30.5	0.5	34	5.8	2.04E-10	3.03E-12	6.0719	0.0900
62	1.0	31	0.5	46	6.8	2.07E-10	3.01E-12	5.9835	0.0869
63	1.0	31.5	0.5	38	6.2	2.10E-10	3.00E-12	5.8980	0.0840
64	1.0	32	0.5	31	5.6	2.13E-10	2.98E-12	5.8155	0.0812
65	1.0	32.5	0.5	42	6.5	2.16E-10	2.96E-12	5.7356	0.0786
66	1.0	33	0.5	35	5.9	2.19E-10	2.95E-12	5.6583	0.0760
67	1.0	33.5	0.5	35	5.9	2.22E-10	2.93E-12	5.5835	0.0736
68	1.0	34	0.5	46	6.8	2.25E-10	2.91E-12	5.5110	0.0713
69	1.0	34.5	0.5	40	6.3	2.28E-10	2.90E-12	5.4408	0.0691
70	1.0	35	0.5	48	6.9	2.31E-10	2.88E-12	5.3728	0.0670
71	1.0	35.5	0.5	41	6.4	2.34E-10	2.86E-12	5.3069	0.0649
72	1.0	36	0.5	33	5.7	2.37E-10	2.84E-12	5.2429	0.0630
73	1.0	36.5	0.5	36	6.0	2.39E-10	2.82E-12	5.1809	0.0611
74	1.0	37	0.5	44	6.6	2.42E-10	2.81E-12	5.1207	0.0593
75	1.0	37.5	0.5	31	5.6	2.45E-10	2.79E-12	5.0623	0.0576
76	1.0	38	0.5	42	6.5	2.48E-10	2.77E-12	5.0055	0.0559
77	1.0	38.5	0.5	31	5.6	2.51E-10	2.75E-12	4.9504	0.0543
78	1.0	39	0.5	32	5.7	2.53E-10	2.73E-12	4.8969	0.0528
79	1.0	39.5	0.5	31	5.6	2.56E-10	2.71E-12	4.8449	0.0513
80	1.0	40	0.5	29	5.4	2.59E-10	2.69E-12	4.7943	0.0499
81	1.0	40.5	0.5	36	6.0	2.61E-10	2.67E-12	4.7451	0.0485
82	1.0	41	0.5	21	4.6	2.64E-10	2.65E-12	4.6973	0.0472
83	1.0	41.5	0.5	28	5.3	2.67E-10	2.63E-12	4.6508	0.0459
84	1.0	42	0.5	34	5.8	2.69E-10	2.61E-12	4.6056	0.0446
85	1.0	42.5	0.5	35	5.9	2.72E-10	2.59E-12	4.5615	0.0434
86	1.0	43	0.5	47	6.9	2.75E-10	2.57E-12	4.5187	0.0423
86.5	1.0	43.25	0.5	93	9.6	2.76E-10	2.56E-12	4.4977	0.0417
87	1.0	43.5	0.5	103	10.1	2.77E-10	2.55E-12	4.4769	0.0412
87.5	1.0	43.75	0.5	52	7.2	2.78E-10	2.54E-12	4.4565	0.0406
88	1.0	44	0.5	43	6.6	2.80E-10	2.53E-12	4.4363	0.0401
89	1.0	44.5	0.5	37	6.1	2.82E-10	2.51E-12	4.3967	0.0390
90	1.0	45	0.5	25	5.0	2.85E-10	2.48E-12	4.3582	0.0380
91	1.0	45.5	0.5	34	5.8	2.87E-10	2.46E-12	4.3207	0.0371
92	1.0	46	0.5	33	5.7	2.90E-10	2.44E-12	4.2841	0.0361
93	1.0	46.5	0.5	39	6.2	2.92E-10	2.42E-12	4.2485	0.0352
94	1.0	47	0.5	41	6.4	2.94E-10	2.40E-12	4.2137	0.0343
95	1.0	47.5	0.5	43	6.6	2.97E-10	2.37E-12	4.1799	0.0334

Table 5: Data for x-rays attenuated by an acrylic slide.

2θ	u(2θ)	θ	u(θ)	Count	u(Count)	λ (m)	u(λ) (m)	Energy (keV)	u(Energy) (keV)
96	1.0	48	0.5	35	5.9	2.99E-10	2.35E-12	4.1469	0.0326
97	1.0	48.5	0.5	42	6.5	3.02E-10	2.33E-12	4.1147	0.0318
98	1.0	49	0.5	59	7.7	3.04E-10	2.30E-12	4.0833	0.0310
98.5	1.0	49.25	0.5	162	12.7	3.05E-10	2.29E-12	4.0679	0.0306
99	1.0	49.5	0.5	403	20.1	3.06E-10	2.28E-12	4.0527	0.0302
99.5	1.0	49.75	0.5	365	19.1	3.07E-10	2.27E-12	4.0377	0.0298
100	1.0	50	0.5	87	9.3	3.08E-10	2.26E-12	4.0229	0.0295
100.5	1.0	50.25	0.5	31	5.6	3.10E-10	2.25E-12	4.0083	0.0291
101	1.0	50.5	0.5	35	5.9	3.11E-10	2.23E-12	3.9938	0.0287
102	1.0	51	0.5	31	5.6	3.13E-10	2.21E-12	3.9654	0.0280
103	1.0	51.5	0.5	30	5.5	3.15E-10	2.19E-12	3.9378	0.0273
104	1.0	52	0.5	40	6.3	3.17E-10	2.16E-12	3.9108	0.0267
105	1.0	52.5	0.5	29	5.4	3.19E-10	2.14E-12	3.8844	0.0260
106	1.0	53	0.5	28	5.3	3.22E-10	2.11E-12	3.8587	0.0254
107	1.0	53.5	0.5	32	5.7	3.24E-10	2.09E-12	3.8337	0.0248
108	1.0	54	0.5	27	5.2	3.26E-10	2.07E-12	3.8092	0.0242
109	1.0	54.5	0.5	46	6.8	3.28E-10	2.04E-12	3.7854	0.0236
110	1.0	55	0.5	27	5.2	3.30E-10	2.02E-12	3.7621	0.0230
111	1.0	55.5	0.5	29	5.4	3.32E-10	1.99E-12	3.7394	0.0224
112	1.0	56	0.5	33	5.7	3.34E-10	1.96E-12	3.7172	0.0219
113	1.0	56.5	0.5	23	4.8	3.36E-10	1.94E-12	3.6956	0.0213
114	1.0	57	0.5	27	5.2	3.38E-10	1.91E-12	3.6745	0.0208
115	1.0	57.5	0.5	38	6.2	3.40E-10	1.89E-12	3.6540	0.0203
116	1.0	58	0.5	29	5.4	3.41E-10	1.86E-12	3.6339	0.0198
117	1.0	58.5	0.5	32	5.7	3.43E-10	1.84E-12	3.6143	0.0193
118	1.0	59	0.5	33	5.7	3.45E-10	1.81E-12	3.5952	0.0189
119	1.0	59.5	0.5	39	6.2	3.47E-10	1.78E-12	3.5766	0.0184
120	1.0	60	0.5	38	6.2	3.49E-10	1.76E-12	3.5585	0.0179

Table 6: Data for x-rays attenuated by an acrylic slide.